Toward an Alkene Hydroamination Catalyst: Static and Dynamic ab Initio DFT Studies

Hans Martin Senn,*,† Peter E. Blöchl,‡ and Antonio Togni†

Contribution from the Laboratory of Inorganic Chemistry, Swiss Federal Institute of Technology, ETH Zentrum, CH-8092 Zürich, Switzerland, and the Zürich Research Laboratory, IBM Research Division, CH-8803 Rüschlikon, Switzerland

Received July 29, 1999. Revised Manuscript Received December 28, 1999

Abstract: The catalytic hydroamination of alkenes via alkene activation and subsequent nucleophilic attack has been investigated with Car−Parrinello ab initio molecular-dynamics calculations using the projector-augmented wave method. The complete cycle including all intermediates and transition states was studied with d^8 transition-metal complexes of the type $\{MCl(PH_3)_2\}^{z+}$ (M = Co, Rh, Ir [$z = 0$] and Ni, Pd, Pt [$z = 1$]) as catalysts, comparing the different metals for their suitability. For group 9, nucleophilic attack was identified as the rate-determining step, while the cleavage of the M−C bond is rate-determining for group 10. Overall, group 10 is more favorable than group 9. In particular, nickel complexes were found to be the best-suited potential catalysts with an activation barrier for the rate-determining step of 108 kJ mol^{-1}. β-Hydride elimination as a competing side reaction was found to be kinetically competitive, but thermodynamically disfavored.

Introduction

Amines are a highly valuable class of compounds, both as end products and as versatile intermediates in many industrially relevant processes.[1] One of the most elegant and efficient approaches to their synthesis is the hydroamination of alkenes (Scheme 1): The formal addition of the N−H bond of an amine across the alkene C=C double bond yields alkylated amines in a direct, 100% atom-economic process from readily accessible starting materials.

From a thermodynamic standpoint, this reaction is feasible:[2] it is exergonic and exothermic under standard conditions. The entropy of reaction, however, is negative. This precludes the use of elevated temperatures to overcome the high activation barrier that prevents the direct addition reaction at room temperature. Hence, a catalyst is required to open an alternative, low-energy pathway. A variety of catalysts have been used, such as bases, acids, and different metal complexes containing transition or lanthanide metals; the topic has been extensively reviewed,[1−8] most recently by Müller and Beller.[9] We therefore mention only a few selected examples involving metal complexes, illustrating the current scope.

Scheme 1. Hydroamination of Alkenes

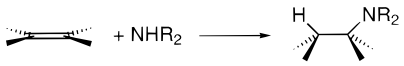

Rhodium complexes have been reported by Brunet and co-workers[10−12] to catalyze the hydroamination of styrene with aniline. The rhodium-catalyzed anti-Markovnikov addition of aromatic and secondary aliphatic amines to styrene and other aromatic alkenes has very recently been described by Beller and co-workers.[13−15] Casalnuovo et al.[16] investigated an iridium complex working as catalyst for the hydroamination of norbornene with aniline via N−H activation, although with a very low activity. Also using iridium complexes, we have developed the first enantioselective intermolecular alkene hydroamination[17] as well as its intramolecular variant.[18] Marks and co-workers achieved both the intramolecular[19−23] (also enantioselectively[24])

* To whom correspondence should be addressed. E-mail senn@inorg.chem.ethz.ch.

† ETH Zürich.

‡ IBM Research Division.

(1) Brunet, J.-J.; Neibecker, D.; Niedercorn, F. *J. Mol. Catal.* **1989**, *49*, 235−259.

(2) Steinborn, D.; Taube, R. *Z. Chem.* **1986**, *26*, 349−359.

(3) Gasc, M. B.; Lattes, A.; Perie, J. J. *Tetrahedron* **1983**, *39*, 703−731.

(4) Roundhill, D. M. *Chem. Rev.* **1992**, *92*, 1−25.

(5) Savoia, D. In *Stereoselective Synthesis*; Methods of Organic Chemistry (Houben-Weyl), 4th ed., Workbench Edition E21; Helmchen, G., Hoffmann, R. W., Mulzer, J., Schaumann, E., Eds.; Thieme: Stuttgart, 1996; Vol. 9, pp 5356−5394.

(6) Taube, R. In *Applied Homogeneous Catalysis with Organometallic Compounds*; Cornils, B., Herrmann, W. A., Eds.; VCH: Weinheim, 1996; Vol. 1, pp 507−520.

(7) Brunet, J.-J. *Gazz. Chim. Ital.* **1997**, *127*, 111−118.

(8) Roundhill, D. M. *Catal. Today* **1997**, *37*, 155−165.

(9) Müller, T. E.; Beller, M. *Chem. Rev.* **1998**, *98*, 675−703.

(10) Brunet, J.-J.; Neibecker, D.; Philippot, K. *J. Chem. Soc., Chem. Commun.* **1992**, 1215−1216.

(11) Brunet, J.-J.; Neibecker, D.; Philippot, K. *Tetrahedron Lett.* **1993**, *34*, 3877−3880.

(12) Brunet, J.-J.; Commenges, G.; Neibecker, D.; Philippot, K. *J. Organomet. Chem.* **1994**, *469*, 221−228.

(13) Beller, M.; Thiel, O. R.; Trauthwein, H. *Synlett* **1999**, 243−245.

(14) Beller, M.; Trauthwein, H.; Eichberger, M.; Breindl, C.; Herwig, J.; Müller, T. E.; Thiel, O. R. *Chem. Eur. J.* **1999**, *5*, 1306−1319.

(15) Beller, M.; Trauthwein, H.; Eichberger, M.; Breindl, C.; Müller, T. E. *Eur. J. Inorg. Chem.* **1999**, 1121−1132.

(16) Casalnuovo, A. L.; Calabrese, J. C.; Milstein, D. *J. Am. Chem. Soc.* **1988**, *110*, 6738−6744.

(17) Dorta, R.; Egli, P.; Zürcher, F.; Togni, A. *J. Am. Chem. Soc.* **1997**, *119*, 10857−10858.

(18) (a) Bieler, N.; Egli, P.; Dorta, R.; Togni, A.; Eyer, M. European Patent Application EP 0 909 762 A2, 1999; *Chem. Abstr.* **1999**, *130*, 305622. (b) Dorta, R.; Egli, P.; Bieler, N. H.; Togni, A.; Eyer, M. U.S. Patent 5,929,265, 1999.

(19) Gagné, M. R.; Marks, T. J. *J. Am. Chem. Soc.* **1989**, *111*, 4108−4109.

(20) Gagné, M. R.; Nolan, S. P.; Marks, T. J. *Organometallics* **1990**, *9*, 1716−1718.

(21) Gagné, M. R.; Stern, C. L.; Marks, T. J. *J. Am. Chem. Soc.* **1992**, *114*, 275−294.

(22) Gagné, M. R.; Brard, L.; Conticello, V. P.; Giardello, M. A.; Stern, C. L.; Marks, T. J. *Organometallics* **1992**, *11*, 2003−2005.

10.1021/ja992689h CCC: $19.00
Published on Web 04/14/2000

Scheme 2. Main Mechanistic Pathways for Hydroamination Catalyzed by a Metal Complex [M]: (a) C═C Activation and (b) N−H Activation

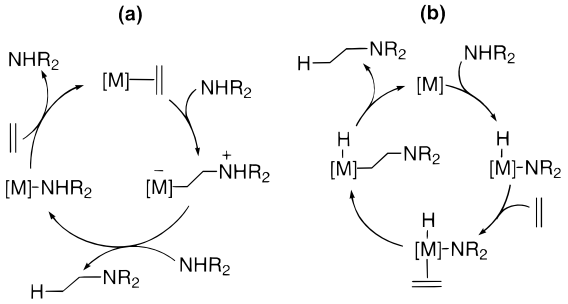

and the intermolecular[25] hydroamination of alkenes catalyzed by lanthanide complexes, which has been extended by Molander and Dowdy.[26,27]

Reports on the use of group 10 metals are scarce. Nickel in the presence of phosphanes and protic acid was shown to catalyze the hydroamination of norbornadiene with morpholine or piperidine,[28] and Seligson and Trogler[29] reported a palladium/phosphane system catalyzing the addition of aniline to activated alkenes with cocatalytic amounts of H^+.

Despite the various developments achieved over the years, there is still no efficient, generally applicable catalytic system available. We have therefore decided to embark on a theoretical study to investigate systematically a series of transition-metal complexes for their suitability as hydroamination catalysts using state-of-the-art static and dynamic DFT methods.

2. Mechanistic Considerations and a Model System

The two principal mechanistic pathways to be considered for hydroamination involve either activation of the amine or activation of the alkene, the latter being the scope of this paper. Amine activation (Scheme 2b) proceeds via oxidative addition of the amine N−H bond to the coordinatively unsaturated metal center, forming an amido hydrido complex, followed by alkene coordination, insertion of the alkene into the metal−nitrogen bond, and finally C−H reductive elimination, liberating the product and closing the catalytic cycle. In the iridium system by Casalnuovo et al.,[16] the intermediate hydrido alkyl complex resulting from alkene insertion could be isolated and structurally characterized.

In the alkene activation mechanism (Scheme 2a), the C═C double bond is activated by coordination to the metal, and the C−N bond is formed by nucleophilic attack of the amine on the coordinated alkene. To liberate the product, the metal−carbon bond in the resulting ammonioalkyl complex has to be cleaved. This can be brought about either by direct protonolysis or by protonation at the metal center with subsequent C−H reductive elimination. The remaining amine complex finally undergoes ligand exchange with a new alkene, regenerating the starting complex. Experimental evidence for this general mechanism is provided by the palladium/phosphane system,[29] where the ammonioalkyl complex as immediate product of nucleophilic attack was detected NMR-spectroscopically, and the need for 1 equiv of protons[29] supports protonolytic M−C cleavage. In addition, the activation of a coordinated alkene toward nucleophilic attack[30] by an amine is well documented for palladium[31,32] and platinum.[33−35]

Scheme 3. C═C Activation Cycle and Model Complexes

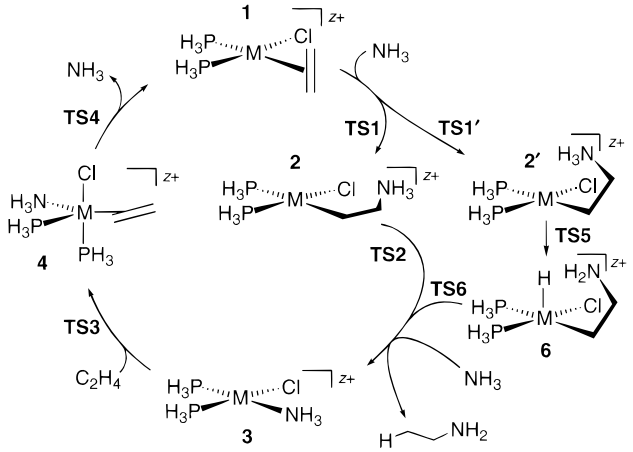

	a	b	c	d	e	f
M	Co	Rh	Ir	Ni	Pd	Pt
z	0	0	0	1	1	1

From the theoretical point of view, the bonding of ethene and its reactivity toward attack by amines were studied at the HF level by Åkermark et al.[36] for nickel(0) and nickel(II) complexes of the type $[NiL_2(C_2H_4)]^{0,2+}$ (L = H_2O, NH_3, PH_3) and $[NiX_2(C_2H_4)]$ (X = F, Cl, CH_3, CN, NH_2), respectively; they found that a cationic complex is required to activate the alkene. A similar study,[37] also at the HF level, for palladium(II) complexes of the type $[PdF_nL_{3-n}(C_2H_4)]^{2-n}$ (n = 1, 2, 3; L = NH_3, PH_3) came to the same conclusion and additionally pointed out the beneficial effect of soft ligands such as PH_3.

In this study, we have focused on the C═C activation pathway, while N−H activation will be dealt with in a forthcoming contribution.[38] The cycle and corresponding model complexes are shown in Scheme 3. It is to be noted that the seemingly simple complexes of type **1** are surprisingly poorly characterized species, particularly with group 10 metals; for example, no crystal structure of such a complex has been reported.[39] We have investigated intermediates and transition states for the complete cycle with d^8-transition-metal complexes from groups 9 and 10. While keeping electron count and ancillary ligands constant, we systematically varied the metal

(23) Tian, S.; Arredondo, V. M.; Stern, C. L.; Marks, T. J. *Organometallics* **1999**, *18*, 2568−2570.
(24) Giardello, M. A.; Conticello, V. P.; Brard, L.; Gagné, M. R.; Marks, T. J. *J. Am. Chem. Soc.* **1994**, *116*, 10241−10254.
(25) Li, Y.; Marks, T. J. *Organometallics* **1996**, *15*, 3770−3772.
(26) Molander, G. A.; Dowdy, E. D. *J. Org. Chem.* **1998**, *63*, 8983−8988.
(27) Molander, G. A.; Dowdy, E. D. *J. Org. Chem.* **1999**, *64*, 6515−6517.
(28) Kiji, J.; Nishimura, S.; Yoshikawa, S.; Sasakawa, E.; Furukawa, J. *Bull. Chem. Soc. Jpn.* **1974**, *47*, 2523−2525.
(29) Seligson, A. L.; Trogler, W. C. *Organometallics* **1993**, *12*, 744−751.
(30) Åkermark, B.; Bäckvall, J.-E.; Zetterberg, K. *Acta Chem. Scand. B* **1982**, *36*, 577−585.
(31) Åkermark, B.; Bäckvall, J.-E.; Hegedus, L. S.; Zetterberg, K.; Siirala-Hansén, K.; Sjöberg, K. *J. Organomet. Chem.* **1974**, *72*, 127−138.
(32) Hegedus, L. S.; Åkermark, B.; Zetterberg, K.; Olsson, L. F. *J. Am. Chem. Soc.* **1984**, *106*, 7122−7126.
(33) Panunzi, A.; De Renzi, A.; Palumbo, R.; Paiaro, G. *J. Am. Chem. Soc.* **1969**, *91*, 3879−3883.
(34) Panunzi, A.; De Renzi, A.; Paiaro, G. *J. Am. Chem. Soc.* **1970**, *92*, 3488−3489.
(35) Benedetti, E.; De Renzi, A.; Paiaro, G.; Panunzi, A.; Pedone, C. *Gazz. Chim. Ital.* **1972**, *102*, 744−754.
(36) Åkermark, B.; Almemark, M.; Almlöf, J.; Bäckvall, J.-E.; Roos, B. O.; Støgård, Å. *J. Am. Chem. Soc.* **1977**, *99*, 4617−4624.
(37) Sakaki, S.; Maruta, K.; Ohkubo, K. *Inorg. Chem.* **1987**, *26*, 2499−2505.
(38) Senn, H. M.; Blöchl, P. E.; Togni, A. In preparation.

center. The complexes contained the common moiety $\{MCl(PH_3)_2\}^{z+}$ with M = Ni(II), Pd(II), Pt(II) ($z = 1$) and Co(I), Rh(I), Ir(I) ($z = 0$); in view of the use of chiral, bidentate phosphane ligands, we kept the two phosphanes always in the cis configuration. This approach enabled us to assess each metal's propensity to act as a catalyst for hydroamination. We will first present the main features of the full reaction profiles for all metals and then proceed stepwise through the cycle, discussing geometric and electronic aspects of intermediates and transition states for individual steps.

3. Computational Details

All reported calculations were carried out with the PAW (projector-augmented wave) method, an all-electron Car−Parrinello[40] ab initio molecular-dynamics code developed by one of us.[41] The wave functions were expanded into augmented plane waves up to a cutoff energy of 30 Ry, the density up to 60 Ry. The frozen-core approximation was employed for the corresponding next-lower noble-gas shell, i.e., a [He] core for C and N, [Ne] for P and Cl, [Ar] for Co and Ni, [Kr] for Rh and Pd, and [Xe] for Ir and Pt. Periodic boundary conditions were used, with an fcc unit cell spanned by the lattice vectors [0.0,9.0,9.0], [9.0,0.0,9.0], [9.0,9.0,0.0] (in Å). To prevent electrostatic interactions between the periodic images, a charge separation scheme[42] was used. The calculations were done within the local-density approximation as parametrized by Perdew and Wang,[43] with gradient corrections for exchange and correlation due to Becke[44] and Perdew,[45,46] respectively. For minimizations, atomic masses were rescaled to 2 (H) and 5 u (all other atoms); a time step of 20 au (0.48 fs) and a fictitious mass for the wave functions of 4000 au were used. True masses, a time step of 10 au, and a fictitious mass of 1000 au were used in free dynamics simulations.

Transition states (TS) were localized using constrained dynamics, where one degree of freedom was chosen as the reaction coordinate (RC) and continuously varied by means of a one-dimensional constraint (e.g., a bond distance). The system was then fully relaxed at fixed values of the RC to locate exactly the position of the TS. Dynamical reaction paths were obtained by starting dynamics simulations from the TS.

Details on the augmentation, charge decoupling, and the reaction coordinates used are provided as Supporting Information. See ref 47 for details on constraints, TS localization, and dynamical reaction paths.

Results and Discussion

A. Complete Reaction Profile. The reaction profiles for catalytic hydroamination via C═C activation/external nucleophilic attack (Scheme 3) with group 9 and group 10 complexes are collected in Figure 1, the corresponding energies of reaction and of activation in Table 1. Assessing the profiles for their suitability in a catalytic process, one should take into account the following general criteria: (1) The overall reaction should be exothermic or thermoneutral; (2) the maximum activation energy should not be higher than 130 kJ mol^{-1};[48] and (3) there should be no very low-lying intermediate. These features correspond to a "flat" profile which ensures that the catalytic cycle is neither blocked by a prohibitive barrier nor trapped in a thermodynamic sink.

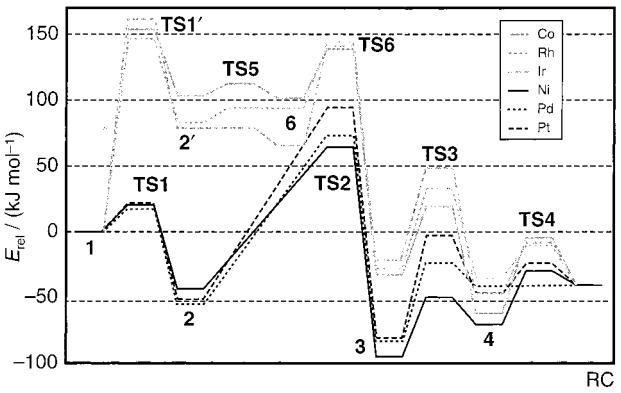

Figure 1. Complete reaction profiles for catalytic hydroamination according to Scheme 3 with group 9 and group 10 metal complexes.

Table 1. Reaction and Activation Energies According to Scheme 3

	Δ_rE or $\Delta E^{\ddagger}$/(kJ mol^{-1})[a]					
step	Co	Rh	Ir	Ni	Pd	Pt
1 → **2**, **2′**	*154*	*147*	*161*	*21*	*17*	*22*
	103	83	79	−44	−55	−52
2′ → **6**	*9*	*11*	*0.2*			
	−2	11	−13			
2, **6** → **3**	*37*	*50*	*75*	*108*	*128*	*146*
	−134	−122	−87	−52	−28	−29
3 → **4**	*2*	*61*	*−25*	*45*	*60*	*78*
	−30	−7	39	24	42	34
4 → **1**	*58*	*25*	*39*	*41*	*−*[b]	*23*
	2	−6	6	30	1	6

[a] For each step, the activation energy $\Delta E^{\ddagger}$ is given in italics, the reaction energy Δ_rE in Roman type. [b] No barrier found.[59]

The hydroamination reaction meets the first condition: The net reaction energy for the formation of ethylamine from ammonia and ethene is calculated as −41 kJ mol^{-1} (the experimental value[49] is $\Delta_rH° = -52$ kJ mol^{-1}).

The second condition is the discriminating one in the cycle under study, because the maximum barriers are rather high in all cases. For group 9 complexes, the rate-determining step is nucleophilic attack, for group 10 it is the cleavage of the M−C bond. The corresponding maximum barriers for group 9 are all higher than those for group 10. For group 9, the lowest maximum barrier is 147 kJ mol^{-1} (with Rh), but only 108 kJ mol^{-1} (with Ni) for group 10. Hence, group 10 is generally favored over group 9, and nickel in particular appears as the best-suited metal. The value of 108 kJ mol^{-1} for the highest activation barrier is reasonably low for the cycle to be a viable possibility in a hydroamination process.

For both groups, no highly stabilized intermediates occur. The "flatness" of the profile, judged by the energy difference between the highest-lying transition state and the most stable intermediate, is again more favorable for group 10.

B. High-Spin vs Low-Spin. As all species under consideration have an even number of electrons, they will have an $S = 0$ low-spin ground state for a sufficiently strong ligand field. However, we explored the stability of the $S = 1$ high-spin configuration for a few complexes involving first transition-row metals because of their intrinsically weak ligand field.

For the triplet states of the ethene complexes of Co and Ni (**1*a**, **1*d**), a tetrahedral minimum geometry was found (Figure

(39) Search in the Cambridge Structural Database (Allen, F. H.; Kennard, O. *Chem. Design Automation News* **1993**, *8*, 31−37), version 5.17 from April 1999.
(40) Car, R.; Parrinello, M. *Phys. Rev. Lett.* **1985**, *55*, 2471−2474.
(41) Blöchl, P. E. *Phys. Rev. B* **1994**, *50*, 17953−17979.
(42) Blöchl, P. E. *J. Chem. Phys.* **1995**, *103*, 7422−7428.
(43) Perdew, J. P.; Wang, Y. *Phys. Rev. B* **1992**, *45*, 13244−13249.
(44) Becke, A. D. *Phys. Rev. A* **1988**, *38*, 3098−3100.
(45) Perdew, J. P. *Phys. Rev. B* **1986**, *33*, 8822−8824.
(46) Perdew, J. P. *Phys. Rev. B* **1986**, *34*, 7406.
(47) Blöchl, P. E.; Senn, H. M.; Togni, A. In *Transition State Modeling for Catalysis*; Truhlar, D. G., Morokuma, K., Eds.; ACS Symp. Ser. 721; American Chemical Society: Washington, DC, 1998; pp 88−99.
(48) This figure is obtained from the following crude estimate: With $\Delta E^{\ddagger} = 130$ kJ mol^{-1}, $T = 373$ K, and $A = 10^{14}$ s^{-1} (corresponding to a typical bond stretch frequency of ∼3000 cm^{-1}), one obtains $k = A \exp\{\Delta E^{\ddagger}/RT\} = 6 \times 10^{-5}$ s^{-1}. Assuming k to be the turnover frequency, it would take approximately 4.5 h for one turnover.
(49) Daubert, T. E.; Danner, R. P. *Physical and Thermodynamic Properties of Pure Chemicals: Data Compilation*; Taylor & Francis: Washington, DC, 1993−.

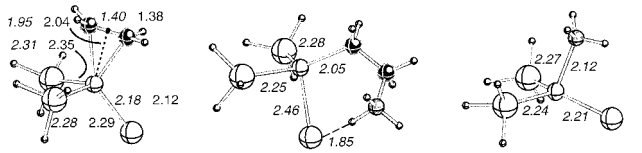

Figure 2. Optimized structures of the high-spin ($S = 1$) complexes. Selected bond lengths are given in Å; the values are arranged in columns according to the periodic table, those for group 9 set in italics, those for group 10 complexes in Roman type.

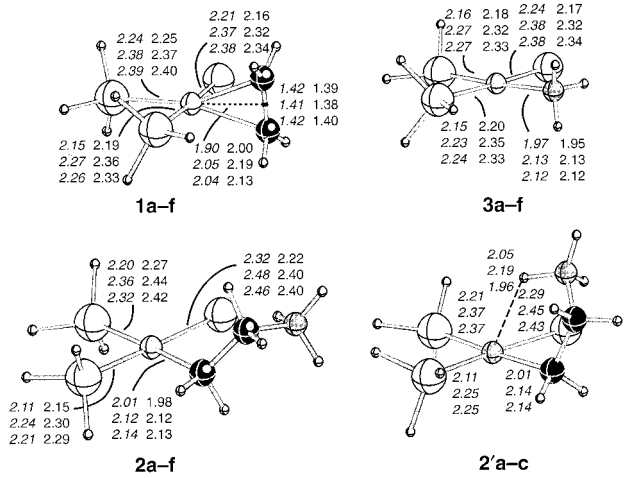

Figure 3. Optimized structures of the alkene, ammonioalkyl, and ammine complexes. See the caption to Figure 2 for explanations.

2). The triplet lies 58 kJ mol^{-1} above the singlet for Ni, and was therefore not considered further. For Co, the high-spin state was found to be 5 kJ mol^{-1} more stable than the singlet. Hence, we also calculated the triplet states of the cobalt ammonioalkyl complex **2*a** and the ammine complex **3*a**. Due to the weak ligand field of the ammine ligand, the latter should exhibit the strongest tendency for a high-spin ground state. However, **2*a** is less stable by 36 kJ mol^{-1} than the corresponding singlet **2′a**, and **3*a** is still destabilized by 14 kJ mol^{-1} relative to the singlet **3a**. In view of these results, we deemed it justified to restrict the remainder of our study to singlet states.

C. Nucleophilic Attack. i. Alkene Complexes. The ethene complexes $[MCl(PH_3)_2(C_2H_4)]^{z+}$ (**1**) adopt the square-planar coordination geometry expected[50,51] for d^8 systems, the C−C axis of the alkene lying perpendicular to the coordination plane (Figure 3). This orientation of the alkene is mainly due to steric reasons;[52,53] electronically, the differences in orbital energy and composition between the two alternative π-donating orbitals on the metal (d_{xz} and d_{xy}) are minor. The only significant deviation from planarity is found for Co, where the alkene is tilted out of the (P, Co, P) plane (P^{trans}−Co−CC 154°[54]). The stronger metal−alkene d−π^* interaction in the group 9 complexes, due to the higher charge density at the metal, is reflected in shorter M−CC and longer C−C distances.

Electronically, the key feature in view of a nucleophilic attack on the alkene is the nature of the vacant orbital acting as acceptor: It consists of the antibonding combination of the alkene π^* orbital with the metal d orbital of matching symmetry (d_{xz}, see Figure 4), i.e., (π^*-d_{xz}). Although this orbital is not the LUMO, but the LUMO+1 (except for Ir),[50] its localization on the alkene carbons makes it the acceptor orbital of choice for the lone pair of an incoming nucleophile.The LUMO is the σ-antibonding combination of metal $d_{x^2-y^2}$ with the alkene π orbital, i.e., ($d_{x^2-y^2}-\pi$). The accepting (π^*-d_{xz}) orbital stays at about constant energy as one moves down within the group, whereas the ($d_{x^2-y^2}-\pi$) orbital rises in energy. For Ir, the ($d_{x^2-y^2}-\pi$) combination lies even higher than (π^*-d_{xz}), and the characters of LUMO and LUMO+1 are thus reversed in **1c**. As the HOMO is also about constant in energy, the HOMO−LUMO gap increases down the group.

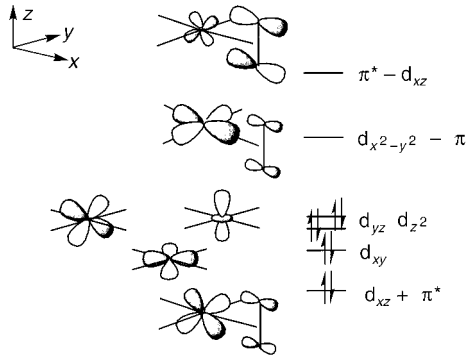

Figure 4. Schematic composition of the highest occupied and lowest unoccupied orbitals for the alkene complexes **1**. The acceptor orbital relevant for nucleophilic attack is (π^*-d_{xz}).

Scheme 4. Changes in Formal Charge upon Nucleophilic Attack for Group 9 and Group 10 Complexes

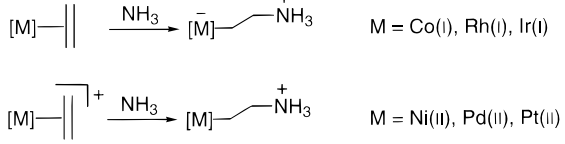

ii. Ammonioalkyl Complexes. The nucleophilic attack of NH_3 on the coordinated ethene yields the ammonioethyl complexes $[MCl(PH_3)_2(CH_2CH_2NH_3)]^{z+}$ (**2**). The reaction is exothermic for Ni, Pd, and Pt ($\Delta_r E = -44, -55, -52$ kJ mol^{-1}), but strongly endothermic for Co, Rh, and Ir ($\Delta_r E = 103, 83, 79$ kJ mol^{-1}). This can be understood in terms of donor and acceptor properties of the ligands involved (Scheme 4): As this reaction step converts an electron accepting alkene into an electron donating alkyl ligand, it is much more favorable for a cationic, relatively electron-poor group 10 complex than for an already electron-rich, neutral group 9 complex. The cationic complexes have a far higher propensity than the neutral ones to accommodate the additional electron density brought into the system through the ammonia lone pair.

For all metals, a minimum conformation could be found in which the positively charged ammonium group points toward the negatively polarized chloro ligand (Figure 3, **2a**−**f**). In the group 9 complexes, however, another, lower-lying minimum corresponds to a bent-back conformation of the $CH_2CH_2NH_3^+$ chain, which places one of the ammonium hydrogens close to the electron-rich metal center (Figure 3, **2′a**−**c**), stabilizing this conformation relative to the former by 16, 18, and 28 kJ mol^{-1} for Co, Rh, and Ir, respectively. For larger ligands, however, such a conformation would be disfavored due to the higher steric demands. No analogous stable conformation could be found for the group 10 complexes.

iii. Transition States for Nucleophilic Attack. In agreement with the electronic considerations sketched above and the

(50) Albright, T. A.; Burdett, J. K.; Whangbo, M.-H. *Orbital Interactions in Chemistry*; Wiley: New York, 1985.
(51) Mingos, D. M. P. In *Comprehensive Organometallic Chemistry*; Wilkinson, G., Stone, F. G. A., Abel, E. W., Eds.; Pergamon: Oxford, 1982; Vol. 3, pp 1−88.
(52) Albright, T. A.; Hoffmann, R.; Thibeault, J. C.; Thorn, D. L. *J. Am. Chem. Soc.* **1979**, *101*, 3801−3812.
(53) Ziegler, T.; Rauk, A. *Inorg. Chem.* **1979**, *18*, 1558−1565.
(54) CC designates the midpoint of the alkene C═C bond.

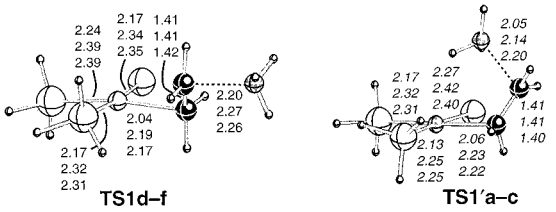

Figure 5. Transition states for nucleophilic attack. See the caption to Figure 2 for explanations.

thermodynamics of the reaction, the barriers for nucleophilic attack are high for Co, Rh, and Ir ($\Delta E^{\ddagger} = 154$, 147, 161 kJ mol^{-1}), but fairly low for Ni, Pd, and Pt ($\Delta E^{\ddagger} = 21$, 17, 22 kJ mol^{-1}). All the orbitals are shifted to lower energies as one goes from the neutral group 9 to the cationic group 10 complexes. The energy gap between the accepting (π^*-d_{xz}) orbital and the NH_3 lone pair is thus reduced, which explains from an electronic standpoint the lower barrier for group 10. Within the groups, the barriers are almost constant, which relates to the constant position of the (π^*-d_{xz}) orbital.

For the group 10 metals, this barrier is the highest overall and therefore rate-determining. The transition states **TS1d**−**f** and **TS1′a**−**c** (Figure 5) for the group 9 and the group 10 complexes, respectively, belong to different trajectories of attack, leading to different conformations of the product complex. The group 10 transition states **TS1d**−**f** connect the alkene complexes **1d**−**f** with the ammonioalkyl complexes **2d**−**f**, while the group 9 transition states **TS1′a**−**c** lead from **1a**−**c** to the bent-back conformers **2′a**−**c**.

We performed dynamical reaction path calculations on the process of nucleophilic attack. For Ni, Pd, and Pt, ammonia attacks from "outside", approaching the coordinated ethene trans to the metal. As the alkene starts interacting with the ammonia, it slips along its axis into an η^1 coordination mode;[55−58] the M−C(α) distance shortens, the C−C distance increases, and the hybridization at the alkene carbon atoms changes from sp^2 to sp^3. Figure 6 shows the total energy as a function of the C−N distance along the trajectory together with snapshot structures. Our results are in accordance with earlier studies by Åkermark et al.[36] (Ni) and Sakaki et al.[37] (Pd).

Despite careful search, we could not find the analogous transition state for the group 10 complexes; no smooth path connecting **1a**−**c** with **2a**−**c** seems to exist. Approaching the ammonia on such a trajectory resulted in a potential energy curve all repulsive with respect to C−N bonding. We identified, however, transition states connecting **1a**−**c** with the lower-energy conformers **2′a**−**c**. These transition states (**TS1′a**−**c**) correspond to a "backside" attack on the alkene, i.e., cis with respect to the metal. They exhibit shorter C−N distances compared to **TS1d**−**f**. It should be noted that larger ligands would interfere with this second path, hindering the cis access of the nucleophile to the alkene, and thus increasing the barrier further or even preventing the reaction altogether.

D. M−C Bond Cleavage. i. Ammine Complexes. The cleavage of the metal−carbon bond, which liberates the alkylated amine as the reaction product (see again Scheme 3), leads to the square-planar ammine complexes $[MCl(PH_3)_2(NH_3)]^{z+}$ (**3**, Figure 3). The cleavage reaction, whose energetics include

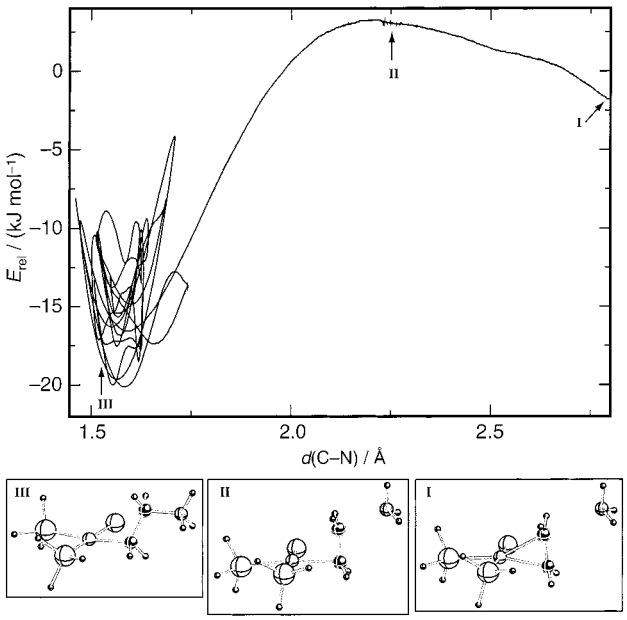

Figure 6. Results from the dynamical reaction path calculation on **TS1d**. The energy is plotted versus the C−N distance as the reaction coordinate, and the snapshot structures illustrate the attack trajectory of the incoming NH_3. Note that the trajectory runs from right to left; at the end point, the C−N distance oscillates around its equilibrium value.

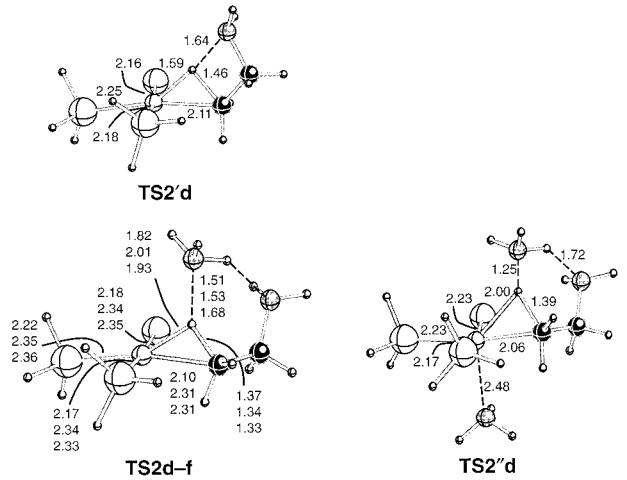

Figure 7. Transition states for protonolysis via intramolecular H transfer (**TS2′**), an intermolecular process with one additional NH_3 (**TS2**), or an intermolecular process with two additional NH_3 (**TS2″**). See the caption to Figure 2 for explanations.

the formation of ethylamine from ammonia and ethene ($\Delta_r E = -41$ kJ mol^{-1}), is quite exothermic for Ni, Pd, and Pt ($\Delta_r E = -51$, −38, −29 kJ mol^{-1}) and very strongly so for Co, Rh, and Ir ($\Delta_r E = -136$, −111, −91 kJ mol^{-1}). The exothermicity decreases in both groups toward the heavier elements. The strong exothermicity for group 9 is due to the ammonioalkyl complexes of these metals being highly unstable. The ammine complexes constitute the most stable species in the reaction profile for group 10.

ii. Transition States for Protonolytic Cleavage. The simplest pathway for M−C protonolysis is an intramolecular process that transfers a proton from the terminal ammonium group to C(α). The corresponding transition state **TS2′d** (Figure 7) was determined for Ni. It exhibits a bridged structure Ni−(μ-H)−C whose Ni−C distance is elongated by 0.13 Å compared to the reactant **2d**. The energy barrier is calculated as $\Delta E^{\ddagger} = 144$ kJ mol^{-1}.

(55) Eisenstein, O.; Hoffmann, R. *J. Am. Chem. Soc.* **1980**, *102*, 6148−6149.
(56) Eisenstein, O.; Hoffmann, R. *J. Am. Chem. Soc.* **1981**, *103*, 4308−4320.
(57) Cameron, A. D.; Smith, V. H., Jr.; Baird, M. C. *Int. J. Quantum Chem., Quantum Chem. Symp.* **1986**, *20*, 657−663.
(58) Cameron, A. D.; Smith, V. H., Jr.; Baird, M. C. *J. Chem. Soc., Dalton Trans.* **1988**, 1037−1043.

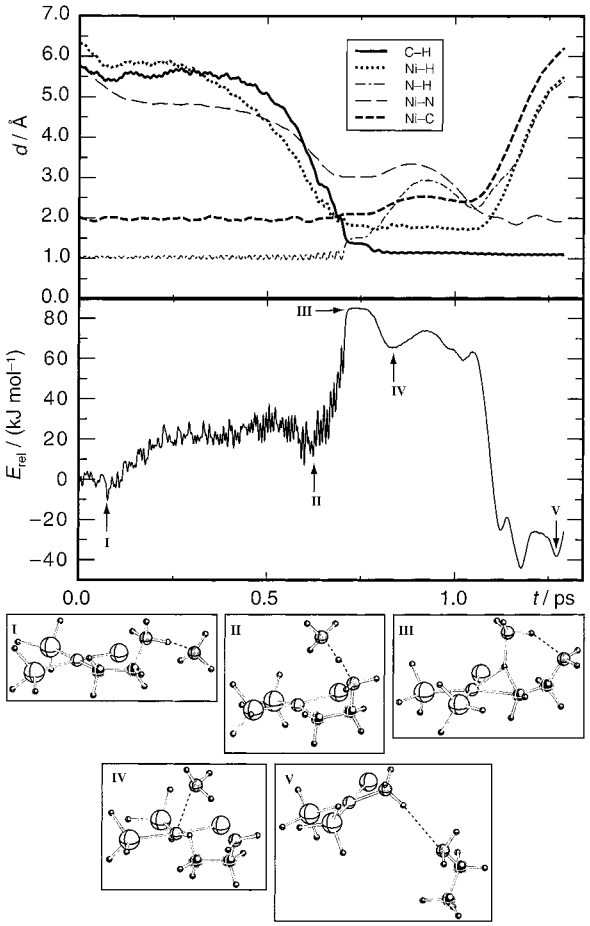

Figure 8. Results from the dynamical reaction path calculation on **TS2d**. Upper graph: Selected bond lengths as a function of time, illustrating the formation and dissociation of the bridged transition state. Lower graph: Energy profile along the path with snapshot structures. The origins of the energy and time scales are chosen arbitrarily.

Because there is always a large excess of amine under catalytic conditions, the proton transfer may very well be an intermolecular process mediated by additional molecules of amine or ammonia, respectively. We investigated two different variants with one and two additional molecules of ammonia.

In the case of one additional NH_3, the proton is transferred from an external NH_4^+ to C(α). This NH_4^+, in turn, is formed by deprotonation of the terminal ammonium group, and the additional molecule of ammonia thus acts as a "proton shuttle". In the transition state (**TS2d**, Figure 7), the proton again bridges the metal−carbon bond. Compared to **TS2′d**, the Ni−H distance is lengthened (1.82 Å vs 1.60 Å), while the N−H and C−H distances are shorter; the Ni−C distance, however, is almost equal. The protonolytic cleavage mechanism was analyzed in detail by dynamical reaction path calculations.[47] After the proton-transfer event, the external NH_3 drifts toward an axial position, coordinates to the metal center, and finally shifts from its axial to the equatorial position, expels the formed ethylamine, still loosely bound to the metal via an agostic interaction, and thus reestablishes a square-planar coordination environment. Figure 8 shows selected bond lengths and the energy profile along the path, together with snapshot structures. The formation and dissociation of the bridged transition state with its transient Ni−H interaction can easily be monitored.

The other group 10 metals behave analogously, exhibiting transition states with qualitatively the same structural features. The barriers are 108, 128, and 146 kJ mol^{-1} for Ni, Pd, and Pt

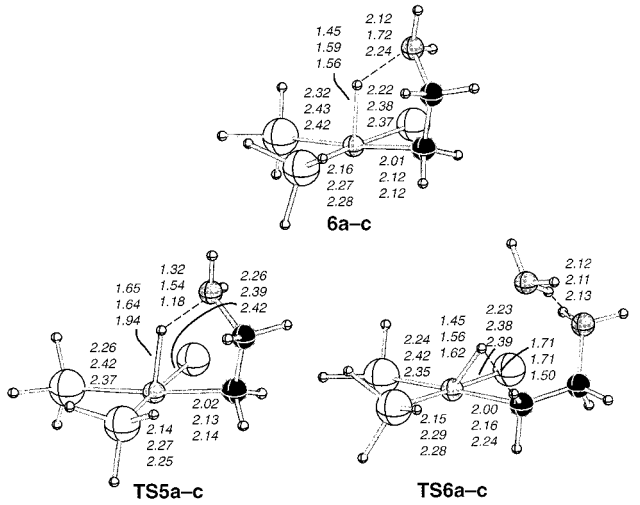

Figure 9. Intermediates and transition states for protonation and subsequent C−H reductive elimination. See the caption to Figure 2 for explanations.

(**TS2d**−**f**). This increase in barrier height from Ni to Pt can be attributed to the increasing stabilization of the principal donor orbital of the metal, the d_{z^2} HOMO. Its interaction with the accepting s orbital of the proton becomes less favorable the lower it lies, thus destabilizing the transition state. The corresponding transition states for the group 9 metals, on the other hand, differ significantly from those of group 10; they belong to a different mechanistic pathway and will be discussed in the next section.

We finally investigated for Ni the protonolysis involving two additional molecules of ammonia. The second NH_3 was placed at an axial position "below" the metal (**TS2″d**, Figure 7), from where it moves to the free equatorial coordination site after the liberation of the product. The double duty fulfilled by the first external NH_3, namely to transfer the proton from the terminal ammonium group onto C(α) and then to saturate the coordination sphere, is here apportioned to two different molecules. However, the barrier increases for this case to $\Delta E^{\ddagger} = 132$ kJ mol^{-1}.

iii. Intermediates and Transition States for Cleavage via Protonation−Reductive Elimination. Locating and analyzing the transition states of type **TS2** for the group 9 complexes, we found them to be transition states for C−H reductive elimination, rather than M−C protonolysis. Hence, for Co, Rh, and Ir, the liberation of the product proceeds not via direct protonolytic cleavage of the M−C bond, but rather through a two-step process, which involves first the formation of a hydride intermediate and subsequently C−H reductive elimination of the product from this hydride.

The hydrido complexes **6a**−**c** (Figure 9) result from the intramolecular protonation of the ammonioalkyl complexes **2′a**−**c**, in which the ammonium group is already suitably oriented toward the metal center such that the proton transfer from the ammonium group to the metal can easily take place. Their structures are almost perfectly square-pyramidal with the aminoalkyl chain in a bent-back conformation such that a stabilizing N−H interaction is still possible. The reaction energies (from **2′a**−**c**) are −2, 11, and −13 kJ mol^{-1} for Co, Rh, and Ir, respectively; the barriers (**TS5a**−**c**) amount to 9.1, 11.2, and 0.2 kJ mol^{-1}. The smoothness with which the protonation at the metal occurs can again be understood in terms of the high electrophilicity of the electron-rich, neutral group 9 complexes. The change in oxidation state from M(I) to M(III)

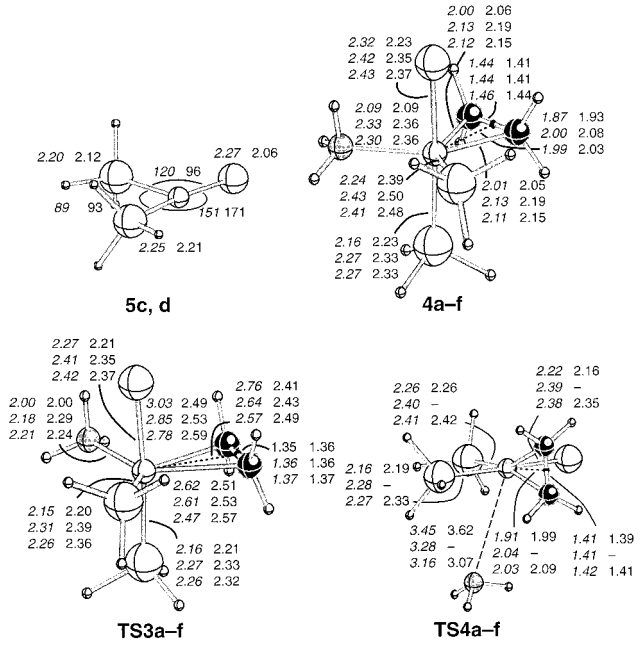

Figure 10. Intermediates and transition states involved in ligand exchange. See the caption to Figure 2 for explanations.

and, concomitantly, from a d^8 to a d^6 species is a favored process for these cases.

From the hydrido complexes **6a**−**c** the ammine complexes **3a**−**c** are formed via the C−H reductive elimination transition states **TS6a**−**c**. The barriers are 37, 50, and 75 kJ mol^{-1} for Co, Rh, and Ir. The reaction is highly exothermic for all three metals, $\Delta_r E = -134, -122, -87$ kJ mol^{-1}.

E. Ligand Exchange. To close the catalytic cycle, the ethene complexes **1** have to be regenerated from the ammine complexes **3**, which corresponds to a ligand exchange of NH_3 by C_2H_4. In principle, either a dissociative mechanism, involving a three-coordinate intermediate, or an associative mechanism, via a pentacoordinate intermediate, are conceivable.

i. Dissociative Pathway. To explore the possibility of a dissociative ligand exchange, the energetics of the three-coordinate species $[MCl(PH_3)_2]^{z+}$ (Figure 10) with M = Ni (z = 1, **5d**) and Ir (z = 0, **5c**) was investigated. The reaction energies from the respective ammine complexes **3d** and **3c** amount to 146 and 98 kJ mol^{-1}. These intermediates being so strongly disfavored, the dissociative mechanism was not further considered. It should be mentioned, however, that the instability of these coordinatively highly unsaturated complexes is overestimated by calculations in the gas phase. In solution, such species will, of course, greatly profit from solvation effects, ion pairing, etc., which make them much more viable than they appear to be in the gas phase. But also in that case, depending on the coordination ability of the solvent, the formation of a solvated unsaturated intermediate with the following displacement of the solvent by the incoming ligand would involve higher-coordinate intermediates or transition states that resemble the five-coordinate species discussed below.

ii. Associative Pathway. Associative ligand exchange proceeds via the pentacoordinate intermediates $[MCl(PH_3)_2(NH_3)(C_2H_4)]^{z+}$ (**4**, Figure 10). They all exhibit the expected trigonal-bipyramidal coordination geometry with the alkene ligand lying in the equatorial plane.[50,51] Their formation from the ammine complexes **3** is endothermic for Ni, Pd, and Pt ($\Delta_r E$ = 24, 42, 34 kJ mol^{-1}) and exothermic for Co, Rh, and Ir ($\Delta_r E = -30, -7, -25$ kJ mol^{-1}). The preference of the neutral group 9 complexes for the coordination of the alkene can again be understood in terms of the stabilization of the electron-rich metal center by the π-accepting alkene ligand, which is also reflected in the lengthening of the C═C bond. These complexes are the most stable species in the whole cycle for the group 9 metals.

The structures of the transition states for alkene coordination **TS3** are shown in Figure 10. The process involves the conversion from square-planar to trigonal-bipyramidal coordination geometry, the transition state being distorted square-pyramidal. The activation energies are fairly similar for the corresponding elements within the row and increase down both groups. They amount to 52, 61, and 70 kJ mol^{-1} for Co, Rh, and Ir and 45, 60, and 78 kJ mol^{-1} for Ni, Pd, and Pt.

In the final step, the five-coordinate complexes **4** lose their ammine ligand, regenerating the alkene complexes **1** and thus closing the catalytic cycle. This step is endothermic for the first-transition-row complexes and almost thermoneutral for second and third row: $\Delta_r E$ = 21, −6, 6; 30, 1, 6 kJ mol^{-1} (Co, Rh, Ir; Ni, Pd, Pt). The barriers amount to 58, 25, and 39 kJ mol^{-1} for Co, Rh, and Ir and 41 and 23 kJ mol^{-1} for Ni and Pt.[59]

F. β-Hydride Elimination from the Ammonioalkyl Complexes. Instead of M−C bond cleavage, the ammonioalkyl complexes **2** can undergo β-hydride abstraction, affording enamine hydrido complexes **7**. After dissociation, the enamine will tautomerize to the more stable imine, and hence, this pathway leaves the hydroamination cycle. As a side reaction competing with hydroamination, we have explored it only for the nickel system, which has appeared to be the best potential catalyst from the screening studies. The formation of imines from alkenes and amines (oxidative amination) catalyzed by cationic rhodium complexes has been described by Beller and co-workers.[13−15,60,61]

i. Enammonium Hydrido Complexes. The primary product of β-hydride elimination from the square-planar (SP) nickel 2-ammonioethyl complex **2d** is a five-coordinate enammonium hydrido complex **7d**. We have calculated energies and structures for all isomers of **7d**, wherein the phosphanes are cis to each other (modeling a chelating bidentate ligand) and the C═C bond of the enammonium lies in the equatorial plane to maximize back-bonding interaction with the metal center.[50] For each of the three positional isomers, all orientations of the enammonium were considered, giving rise to the 10 isomers **7d^1**−**7d^{10}** (Figure 11, Table 2). β-Hydride elimination is endothermic in all cases, the reaction energy varying between 46 (**7d^2**) and 175 kJ mol^{-1} (**7d^8**). Rotating the enamine in **7d^2** about the C═C axis yields **7d^1**, by 56 kJ mol^{-1} less stable. This energy difference is entirely due to the loss of electrostatic stabilization between the positively charged ammonium group and the negatively polarized chloro ligand. The same kind of stability difference is also observed in **7d^7**/**7d^8** and **7d^9**/**7d^{10}**.

Deprotonating the enammonium complex to the corresponding enamine complex by NH_3 is unfavorable for all isomers (Table 2), with endothermicities ranging from 33 (**7d^8**) to 101 kJ mol^{-1} (**7d^3**). For a comparison, deprotonation of the ammonioethyl complex **2d** to the aminoethyl complex costs 169 kJ mol^{-1}. For the four isomers with axial chloride and equatorial hydride (**7d$^{7-10}$**), the enamine complex is not even stable, but rearranges to a 2-iminioethyl complex.

(59) Despite careful search, no transition state could be located for the dissociation of NH_3 from the five-coordinate complex in the case of Pd. The force on the Pd−N bond was negative (attractive) over the whole interval of Pd−N distances searched (up to 4.7 Å); concurrently, the total energy was monotonically rising.

(60) Beller, M.; Eichberger, M.; Trauthwein, H. *Angew. Chem.* **1997**, *109*, 2306−2308; *Angew. Chem., Int. Ed. Engl.* **1997**, *36*, 2225−2227.

(61) Beller, M.; Trauthwein, H.; Eichberger, M.; Breindl, C.; Müller, T. E.; Zapf, A. *J. Organomet. Chem.* **1998**, *566*, 277−285.

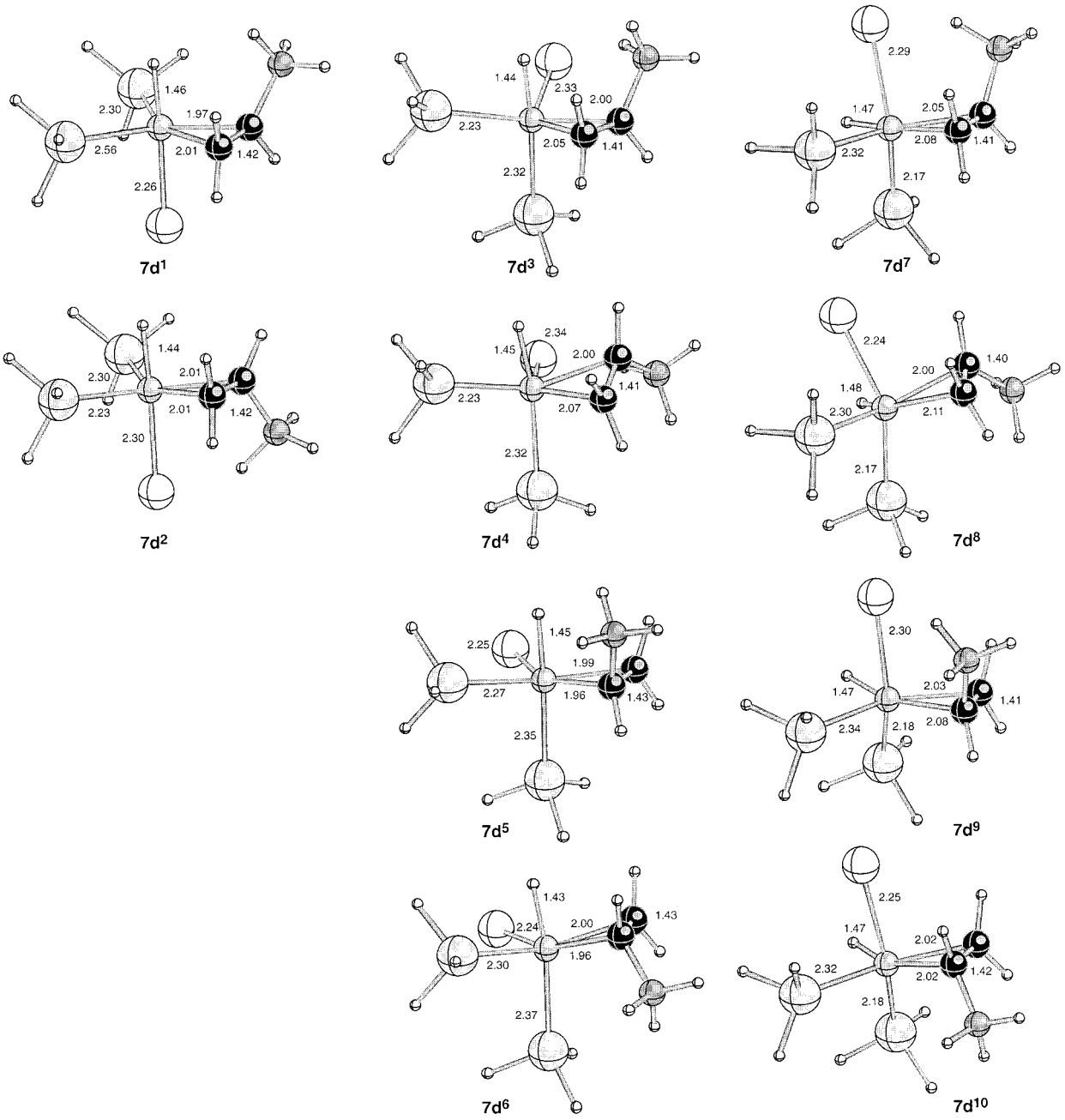

Figure 11. Nickel enammonium hydrido complexes **7d**.

ii. Transition State and Reaction Path for β-Hydride Elimination. β-hydride abstraction in d^8 four-coordinate alkyl complexes or its reverse, alkene insertion into a metal−hydride bond in pentacoordinate complexes, has been the subject of previous theoretical studies.[62−65] The reaction proceeds via a square-pyramidal (SPY) transition state, in which the hydride and the alkene occupy basal positions cis to each other, the alkene C═C axis being oriented within the basal plane. This process involves skeletal rearrangements from the SP reactant to the SPY transition state and from there to the trigonal-bipyramidal (TBPY) product as well as the four-center bond exchange process itself, in which the carbon−hydrogen bond is broken, the metal−hydride bond formed, and the alkyl ligand transformed into a coordinated alkene.

To identify the lowest-energy pathway connecting the ammonioalkyl complex **2d** with one of the enammonium hydrido complexes **7d**, we ran constrained-dynamics simulations from the four most stable isomers of **7d**; the trajectories were validated by full relaxations at fixed values of the reaction coordinate. The most favorable pathway was found from **7d²**, the most stable enammonium hydrido isomer. We localized the corresponding transition state (**TS7d**, Figure 12a) and performed dynamical reaction path calculations to analyze the course of the reaction in more detail (Figure 12b). The barrier for β-hydride elimination from **2d** to **7d²** amounts to 104 kJ mol^{-1}. As the SPY four-center transition state forms from the SP reactant, the β-hydrogen and the β-carbon atoms concurrently bind to the metal center, and the chloride moves into the apical

(62) Hoffmann, R.; Thorn, D. L. *J. Am. Chem. Soc.* **1978**, *100*, 2079−2090.
(63) Koga, N.; Jin, S. Q.; Morokuma, K. *J. Am. Chem. Soc.* **1988**, *110*, 3417−3425.
(64) Koga, N.; Morokuma, K. In *Theoretical Aspects of Homogeneous Catalysis*; van Leeuwen, P. W. N. M., Morokuma, K., van Lenthe, J. H., Eds.; Catalysis by Metal Complexes, Vol. 18; Kluwer: Dordrecht, 1995; pp 65−91.
(65) Versluis, L.; Ziegler, T.; Fan, L. *Inorg. Chem.* **1990**, *29*, 4530−4536.

Table 2. Stabilities (in kJ mol^{-1}) of Enammonium Hydrido and Enamine Hydrido Complexes **7d**

	enammonium form[a]	enamine form[b]
7d^1	102	155
7d^2	46	145
7d^3	82	183
7d^4	102	186
7d^5	136	192
7d^6	148	193
7d^7	98	192[c]
7d^8	175	207[c]
7d^9	101	196[c]
7d^{10}	170	215[c]

[a] Reaction energy for the formation of the enammonium hydrido complex from **2d**. [b] Reaction energy for the formation of the enamine hydrido complex from **2d**, including deprotonation with NH_3 under formation of NH_4^+. [c] Enamine not stable; rearranged to 2-iminioethyl.

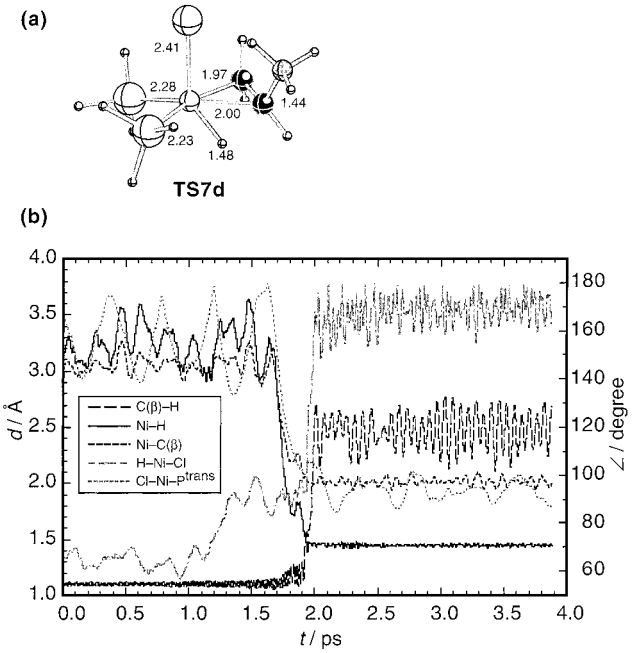

Figure 12. β-Hydride elimination in the ammonioalkyl complex **2d**. (a) Transition state **2d** → **7d^2**. (b) Selected bond lengths and angles as a function of time from a dynamical reaction path calculation, illustrating the skeletal rearrangements SP → SPY → TBPY.

position of the square pyramid. Falling down from the transition state, the system relaxes into the TBPY product structure, while the C−H bond is definitely broken and the hydride swings into the position trans to the chloride.

iii. Assessment of β-Hydride Elimination as a Competing Reaction. β-Hydride elimination in the ammonioalkyl complex **2** leads, as mentioned above, to the formation of imines, and it constitutes therefore an undesired side reaction. In the case of nickel, the barrier of 104 kJ mol^{-1} for β-hydride elimination (**2d** → **7d^2**) is of the same height as the barrier of 108 kJ mol^{-1} for the rate-delimiting protonolytic Ni−C cleavage step (**2d** → **3d**) that liberates the alkylamine. β-Hydride elimination is thus in direct kinetic competition with hydroamination. Thermodynamically, β-hydride elimination is endothermic by 46 kJ mol^{-1}, while protonolytic cleavage is exothermic by −52 kJ mol^{-1}. However, the enammonium hydrido complex is not in equilibrium with the ammonioalkyl complex, because the enammonium will easily dissociate and tautomerize to an imine, leaving a hydrido chloro complex.

To favor hydroamination over β-hydride elimination, one can envisage several strategies: (1) The use of 1,1-disubstituted alkenes affords ammonioalkyl complexes without β-hydrogens, provided the nucleophilic attack of the amine proceeds with Markovnikov selectivity, as usually observed. (2) Since β-hydride elimination involves a pentacoordinate transition state that is more sterically demanding than the SP reactant or the transition state for protonolytic cleavage, bulky ligands impede this pathway, in particular when they protect the free sites above and below the metal center. (3) Preliminary calculations have shown the barrier for β-hydride elimination to be insensitive to electronic ligand effects; using PMe_3 instead of PH_3 does not affect the barrier within ±5 kJ mol^{-1}. However, the enammonium hydrido complex is destabilized by the more electron-donating PMe_3, rendering β-hydride elimination more endothermic (65 kJ mol^{-1}). At the same time, the activation energy for protonolytic cleavage is reduced by electron-donating phosphane ligands,[66] e.g. with PMe_3 to 91 kJ mol^{-1}. Electronic ligand effects thus allow control of the subtle balance between productive protonolytic cleavage and β-hydride elimination by lowering the barrier for cleavage on one hand, and on the other by lowering the barrier for the back-reaction (alkene insertion) by destabilizing the enammonium hydrido species.

Conclusion

State-of-the-art static and dynamic DFT calculations have permitted a plausible and detailed picture of the transition-metal-catalyzed hydroamination of alkenes via C═C activation to be obtained. Intermediates and transition states for the reaction sequence (nucleophilic attack on the coordinated alkene, cleavage of the M−C bond, and ligand exchange) have been studied with d^8 transition-metal complexes of the type $\{MCl(PH_3)_2\}^{z+}$ (M = Co, Rh, Ir [$z = 0$] and Ni, Pd, Pt [$z = 1$]). The differences between group 9 and group 10 complexes have been investigated and analyzed to assess the propensity of the different metals to act as catalysts in hydroamination. The following main conclusions emerged from this study: (i) Nucleophilic attack of the amine on the coordinated alkene is thermodynamically and kinetically favorable for group 10, but strongly disfavored for group 9, where it constitutes the rate-delimiting step. (ii) The cleavage step, on the other hand, is rate-delimiting in the case of group 10, but facile for group 9. For group 10, cleavage proceeds via protonolysis of the metal−carbon bond, involving an M−(μ-H)−C bridged transition state with an additional molecule of ammonia acting as a proton shuttle. For group 9, protonation leads to a hydride intermediate, subsequently undergoing C−H reductive elimination. (iii) Overall, group 10 complexes have appeared to be more suitable. The nickel system in particular has been identified as the most promising potential catalyst with a rate-delimiting activation barrier in the cleavage step of 108 kJ mol^{-1}. (iv) β-Hydride elimination from the ammonioalkyl complex has been studied for nickel as a competing side reaction. It is kinetically competitive with protonolytic cleavage, but thermodynamically disfavored. Using steric and electronic ligand effects or by choice of suitable substrates, β-hydride elimination can be discriminated against protonolytic cleavage or even completely blocked.

In view of the rate-determining nature of the protonolytic cleavage, we have also performed calculations directed toward identifying ligand electronic effects affecting the activation barrier of this step. The influence of phosphanes bearing electron-withdrawing/donating substituents on the energy of the transition state for Ni−C bond cleavage has been studied.[66] With these results in hand, complexes having corresponding properties

(66) Senn, H. M.; Deubel, D. V.; Blöchl, P. E.; Togni, A.; Frenking, G. *J. Mol. Struct. (THEOCHEM).* In press.

shall be prepared and tested as catalysts. We shall report in due course about our search for better catalysts guided by theoretical studies.

Supporting Information Available: Details on the augmentation of the plane waves, parameters used in the charge decoupling scheme, as well as Cartesian coordinates and energy levels of all optimized species (ASCII). This material is available free of charge via the Internet at http://pubs.acs.org/.

JA992689H